Materials Research, Vol. 5, No. 1, 1-11, 2002.

Review Article

Synchrotron SAXS Studies of Nanostructured Materials and Colloidal Solutions. A Review

A.F. Craievich

Institute of Physics, University of São Paulo,
C.P. 66318, 05315-970 São Paulo - SP, Brazil

Received: September 20, 2001; Revised: December 29, 2001

Structural characterisations using the SAXS technique in a number of nanoheterogeneous materials and liquid solutions are reviewed. The studied systems are protein (lysozyme)/water solutions, colloidal ZnO particles/water sols, nanoporous NiO-based xerogels, hybrid organic-inorganic siloxane-PEG and PPG nanocomposites and PbTe semiconductor nanocrystals embedded in a glass matrix. These investigations also focus on the transformations of time-varying structures and on structural changes related to variations in temperature and composition. The reviewed investigations aim at explaining the unusual and often interesting properties of nanostructured materials and solutions. Most of the reported studies were carried out using the SAXS beamline at the National Synchrotron Light Laboratory (LNLS), Campinas, Brazil.

Keywords: *nanoheterogeneous systems, nanostructured materials, SAXS, synchrotron radiation*

1. Introduction

A number of nanostructured materials and colloidal liquid solutions with interesting physical and chemical properties have been recently developed. In order to understand their unusual properties, structural information is generally required. Knowledge about the structural transformations occurring during materials processing is also useful. Because of the nanometric and rather disordered nature of precursors, intermediate materials and final products, their structural characterisation is a challenge for materials scientists.

Depending on the desired resolution of the structural study, different characterisation techniques are commonly used. High-resolution transmission electron microscopy (HRTEM), electron diffraction (ED), wide-angle X-ray scattering (WAXS) and extended X-ray absorption fine structure (EXAFS) yield structural information at an atomic resolution. If the relevant structural features are at a superatomic level, from a few tenth up to about 100 nm, small-angle X-ray scattering (SAXS) and, to a lesser extent, small-angle neutron scattering (SANS) are the most widely used techniques. These techniques provide statistical and overall information averaged in a volume on the order of 1 mm^3. Very local structural analysis can in many cases be performed by TEM, this technique being an extremely useful complement for scattering investigations.

Because of the high dilution of many nanometric phases and/or the often rather short transformation time involved in nanomaterial processing, complete SAXS studies using classical X-ray sources are generally difficult and very time consuming. SAXS beamlines in synchrotron radiation laboratories provide very intense monochromatic X-ray beams that make studies of weak scatterer materials possible and, also, *in situ* analyses of structural transformations with a high time resolution. Besides providing a high photon flux, the white nature of synchrotron radiation emission spectrum allows one to use the effect of anomalous scattering for many useful applications.

This paper reports the characteristics of the new synchrotron radiation facility of the National Synchrotron Light Laboratory (LNLS), Campinas, Brazil, describes its SAXS beamline, recalls the basic scattering theory and reviews a set of SAXS investigations dealing with structure and structural transformations of nanomaterials and colloidal solutions. The studied systems are proteins in solution, suspensions of colloidal particles, nanoporous xerogels, hybrid organic-inorganic nanocomposites and semiconductor nanocrystals embedded in a glass matrix. Most of

e-mail: craievich@if.usp.br

the reported investigations were carried out using the LNLS SAXS beamline.

2. The LNLS Synchrotron Source[1,2]

The National Synchrotron Light Laboratory (LNLS) is located in Campinas in the state of São Paulo State, Brazil, 100 km north from the city of São Paulo. The LNLS staff designed, built and now operates an open synchrotron radiation facility. They also assist the external users of the ten already installed VUV and X-ray beamlines.

The LNLS synchrotron source is composed of a 120 MeV LINAC preinjector, a 500 MeV booster synchrontron injector and a 1.37 GeV electron storage ring. The natural emittance of the source is 100 nmrad, the inicial current is 200 mA and the beam life time at 100 mA is 16 h. The spectrum of the emitted photon flux, with a critical energy Ec = 2.05 keV, is illustrated in Fig. 1.

Design, construction and commissioning of the LNLS synchrotron source and first beamlines were completed by June 1997. Since then, more than 800 research projects have been performed by users coming from a number of Brazilian and foreign institutions. A picture of the synchrotron source and beamlines is shown in Fig. 2.

Information on the characteristics of the LNLS electron storage ring and VUV/X-ray beamlines and on the procedure for user access can be found in the Internet website www.lnls.br.

3. The LNLS SAXS Beamline[3]

The photon beam used in the LNLS SAXS beamline comes from one of the 12 bending magnets of the electron storage ring. The white photon beam is extracted from the ring through a high-vacuum path. After passing through a thin beryllium window, the beam is monochromatized and horizontally focussed by a cylindrically bent and asymmetrically cut silicon single crystal. The focus is located at the detection plane. The reflection plane is (111), the asymmetry angle equal to 10° in condensing mode, the energy range is 6-12 keV (1-2 Å) and the energy resolution: (E/ΔE) is about 1,000 for typical detector-to-sample distances.

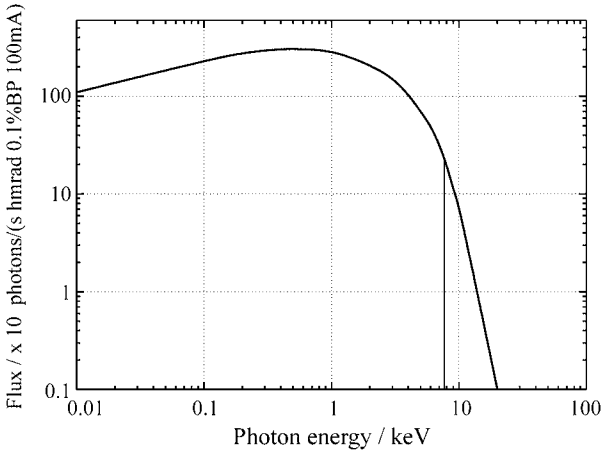

Figure 1. Photon flux emitted by the LNLS 1.37 GeV synchrotron source. The vertical line indicates the energy of the photons (E = 7.85 keV, λ = 1.61 Å) used in typical SAXS experiments at LNLS.

Figure 2. Picture of the LNLS 1.37 GeV synchrotron source (above) and the SAXS beamline (below).

Three sets of slits are used to geometrically define the incoming X-ray beam and suppress most of the parasitic scattering. A vacuum tube from monochromator to detector positions reduces air absorption and scattering. The X-ray photons scattered at small angles are recorded using a one-dimension position-sensitive gas detector, a two-dimension position-sensitive multiwire gas detector or an imaging plate. A schematic layout of the SAXS beamline is shown in Fig. 3.

By using a small incoming beam cross-section and a narrow detection slit, the recorded scattering intensity functions can be kept essentially free from "smearing" effects. Under these conditions, no mathematical desmearing of the experimental SAXS functions is needed.

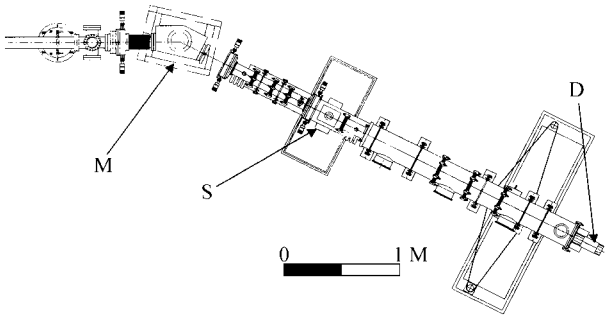

Figure 3. Schematic layout of the LNLS SAXS beamline. The locations of the single crystal monochromator (M), sample holder (S) and detector plane (D) are indicated.

4. Scattering Theory[4]

The X-ray scattering intensity is experimentally determined as a function of the scattering vector q whose modulus is given by $q = (4\pi/\lambda)\sin\theta$, where λ is the X-ray wavelength and θ is half the scattering angle ε (ε: angle between the directions of the scattered and trasmitted beams) . For small angles $q \approx (2\pi/\lambda)\,\varepsilon$.

Macroscopically isotropic systems produce a scattering intensity which only depends on the modulus of q. In the special case of isotropic systems composed of isolated and identical particles embedded in a matrix with a constant electronic density, the normalized SAXS intensity or scattering power I(q) is usually approximated by a product

$$I(q) = N\, I_1(q)\, S(q) \qquad (1)$$

where N is the number of particles per unit volume and $I_1(q)$ is the scattering function of a single isolated particle given by

$$I_1(q) = \int_0^\infty 4\pi\, r^2\, \gamma\,(r)\, \frac{\sin qr}{qr}\, dr \qquad (2)$$

where $\gamma\,(r)$ is the correlation function given by

$$\gamma\,(r) = \left\langle \int_v [\rho\,(\mathbf{r'}) - \rho_0]\,[\rho\,(\mathbf{r'} + \mathbf{r}) - \rho_0]\, d\mathbf{r'} \right\rangle$$

where $\rho(\mathbf{r})$ is the electronic density function inside the particle, ρ_0 is the constant density of the matrix and $\langle\ \rangle$ indicates an averaging for all particle orientations. S(q) is the orientation averaged effective structure function that accounts for the short range spatial correlation between them.

Equation 1 is strictly valid for systems of not very concentrated spheres. It is also generally used as an approximation for anisotropic particles provided the interparticle short range order and the orientational order of each particle are independent. This occurs in real cases when the particles are not very close one from each other.

If the system is "dilute", *i.e.* the particles are far away from each other and without spatial correlation, S(q) = 1 over the whole q range. On the other hand, S(q) = 1 in the high q limit for any system of particles with short-range spatial correlation. Under these conditions, Eq. 1 simply becomes

$$I(q) = N\, I_1(q) \qquad (3)$$

For "two-electronic density systems" consisting of homogeneous particles with a constant electronic density ρ_1 (except the short wavelength modulation associated to individual atoms), and an also homogeneous matrix with a constant density ρ_0, the scattering function for a single particle is given by

$$I_1(q) = (\rho_1 - \rho_0)^2\, v \int_0^{D_{max}} 4\pi\, r^2\, \gamma_0\,(r)\, \frac{\sin qr}{qr}\, dr \qquad (4)$$

where v is the particle volume, D_{max} its maximum dimension and $\gamma_0(r)$ is a function defined by $\langle v(\mathbf{r})\rangle/v$, $\langle v(\mathbf{r})\rangle$ being the orientational average of the intersection between the volume of the particle and the same volume displaced by a vector **r**. The value of the integral only depends on the shape and size of the particle.

Equation 4 implies that the function $I_1(q)$ associated to particles embedded in a homogeneous matrix is equivalent to the same function corresponding to pores of same size and shape as the particles embedded in a homogeneous material, provided the difference in electronic density between both phases $\Delta\rho$ is in both cases the same (Babinet principle).

The distance distribution function of the particle, $p(r)=\gamma_0(r)\, r^2$, can be determined from the scattering function of a single particle by

$$p(r) = \frac{1}{[2\pi^2\,(\rho_1 - \rho_0)^2\, v] \int_0^\infty I_1(q)\, q\, r \sin qr\, dq} \qquad (5)$$

For dilute systems, the function p(r) has positive non-zero values up to a maximum value, D_{max}, corresponding to the largest dimension of the particle.

The function $I_1(q)$ (Eq. 4) has as asymptotic behaviour at small q given by

$$I_1(q) = (\rho_1 - \rho_0)^2\, v^2 e^{-\frac{\langle R_g\rangle_G^2\, q^2}{3}} \qquad (q \to 0) \qquad (6)$$

where v is the particle volume and R_g the radius of gyration of the particles defined by

$$R_g = \left(\frac{1}{v}\int_v r^2\, dv\right)^{1/2} \qquad (7)$$

Equation 3 and 6 lead to the low-q asymptotic scattering function, I(q), corresponding to an isotropic dilute system of N identical particles per unit volume, given by

$$I(q) = N(\rho_1 - \rho_0)^2 v^{\,2}\, e^{-\frac{\langle R_g\rangle_G^2\, q^2}{3}} \qquad (q \to 0) \qquad (8)$$

(Guinier law)

Guinier's law also applies to a dilute system of identical particles with a size distribution. In this case, the parameter $\langle R_g\rangle_G$ corresponds to an average of the radius of gyration, that weighs much more large particles, given by

$$< R_g >_G = \left[\frac{\int [v(R_g)]^2 \, R_g^2 \, G(R_g) \, dR_g}{\int [v(R_g)]^2 \, G(R_g) dR_g} \right]^{\frac{1}{2}}$$

where $G(R_g)$ is the function that defines the size distribution of the particles.

For any isotropic two-electronic density systems, dilute or concentrated (or even for a more general two-phase geometry), the asymptotic behaviour of I(q) at high q is given by Porod's law:

$$I(q) = \frac{2\pi \, (\rho_1 - \rho_0)^2 \, S}{q^4} \qquad (q \to \infty) \tag{9}$$

where S is the surface area of the interface between the two phases. Equation 9 holds for all two-phase systems, provided particles are not very thin disks or cylinders.

In the particular case of a dilute solution of spherical particles with radius R, the scattering function $I_1(q)$ (Eqs. 3 and 4) is given by:

$$I(q) = N \, (\rho_1 - \rho_0)^2 \, v^2 \, [\Phi \, (q)]^2 \tag{10}$$

with $\Phi(q) = [3(\sin qR - qR \sin qR)/(qR)^3]$. This function is characterised by a main maximum at q = 0 and by oscillations at high q with weak secondary maxima located at qR = 5.78, 9.05, ... In the case of identical spherical particles, the asymptotic scattering function at high q oscillates around a curve $I(q) \propto q^{-4}$, as predicted by Eq. 9. These oscillations are damped for systems of spheres having a radius distribution with a small non-zero width and vanish for systems with a wide size distribution.

The scattering function of a dilute set of spherical particles with a radius distribution defined by G(R) is given by

$$I(q) = \int_0^\infty G(R) \, I_1(q) \, dR = (\rho_1 - \rho_0)^2 \int_0^\infty G(R) \, [(4/3) \, \pi \, R^3]^2 \, [\Phi(qR)]^2 dR \tag{11}$$

The function G(R), whose integral is equal to the number of particles per unit volume, N, can be determined from the experimental scattering functions by solving the integral Eq. 11 using a numerical procedure. The most widely used is the GNOM package[5].

An integral property of scattering function that applies to two-density systems is given by

$$Q = \int_0^\infty q^2 \, I(q) \, dq = 2\pi^2 (\rho_1 - \rho_0)^2 \, \phi \, (1 - \phi) \, V \tag{12}$$

where ϕ and $(1-\phi)$ are the respective volume fractions of both phases and V the irradiated volume. For a dilute system of N particles of volume v, Eq. 12 becomes

$$Q = 2 \, \pi^2 \, N \, (\rho_1 - \rho_0)^2 \, v \tag{13}$$

The scattering functions of very concentrated or strongly correlated particle systems exhibit a peak, which is more pronounced and shifts to higher q for increasing particle concentration. For concentrated systems, Eq. 3 does not apply. Instead, under the conditions specified in Section 4, Eq. 1 can be used to fit experimental results and so to determine the relevant structural parameters. Generally, the analysis of the results of scattering measurements of spatially correlated systems is rather difficult, particularly when both, the single particle scattering function $I_1(q)$ and structure function S(q), are not known. One of the difficulties arising in data analysis is to establish the actual origin of the peak. The question to be answered is: Does the maximum correspond to $I_1(q)$ (particles with a complex non-constant electron density), to S(q) (concentrated system of correlated particles) or to both functions?

In the particular case of nearly homogeneous particles, the peaked shape of I(q) corresponds to the structure function S(q). Semiquantitative analysis of scattering data yields a structural parameter, d_s, corresponding to the average distance between particles, given by

$$d_s = \frac{2\pi}{q_m} \tag{14}$$

where q_m is the q value corresponding to the maximum of scattering intensity. Equation 14 is not an exact equation for disordered system because the average distance also depends on the particular type of arrangement around each particle [4]. Nevertheless it can be applied as a useful semiquantitative estimate in order to characterise trends in structural transformations.

A particular case of a correlated particle system is that in which primary particles build up a so-called fractal object. The structure function associated to this system is given by[6]

$$S(q) = 1 + \frac{1}{(qa)^D} \frac{D \, \Gamma \, (D - 1)}{(1 + 1/q^2 \, \xi^2)^{\frac{(D-1)}{2}}} \times \sin[(D - 1) \tan^{-1} (q \, \xi)] \tag{15}$$

where *a* is the radius of the (assumed spherical) primary particles, ξ is the correlation length or size parameter of the fractal object, D is the fractal dimension of the structure and Γ is the gamma function.

If primary particles that build up the fractal object are very small ($a << \xi$), the single particle scattering function $I_1(q)$ of Eq. 6 can be approximated by a constant value

$$I_1(q) = (\rho_1 - \rho_0)^2 v^2 \quad (16)$$

Assuming the composite material consisting of N fractal objects per unit volume, without spatial correlation between them, and that each fractal aggregate is composed of very small primary particles ($a << \xi$) of volume v, the scattering intensity (Eq. 1) is given by

$$I(q) = N(\rho_1 - \rho_0)^2 v^2 S(q) \propto S(q) \quad (17)$$

where S(q) is the intra-aggregate structure function defined by Eq. 15 and N is the number of fractal objects per unit volume. Within the range $1/\xi < q << 1/a$, Eq. 17 becomes a simple power law.

$$I(q) \propto q^{-D} \quad (18)$$

For q values close to or larger than 1/a, the assumption of a constant value for the scattering function of a primary particle (Eq. 16) is not acceptable. Using a better approximation for the single particle scattering function $I_1(q)$, the scattering intensity eventually reaches the asymptotic Porod range and so becomes proportional to q^{-4} (Eq. 9).

At small q ($q \leq 1/\xi$), I(q) exhibits a Guinier-type behaviour (Eq. 8) and therefore the radius of gyration of the isolated fractal aggregates, R_g, can easily be determined from experimental results. This parameter is related to the correlation length ξ of the fractal objets by

$$R_g = [D(D + 1)/2]^{1/2} \xi \quad (19)$$

The equations mentioned in this section can be considered as the basic background needed to understand procedures often used to infer low-resolution (superatomic) structural information from experimental scattering data. These equations will be applied and referred in the different SAXS investigations of nanoheterogeneous materials to be reported in section 5.

5. Structural Investigations of Nanostructured Systems

5.1. Protein (lysozyme) unfolding process[7]

The atomic structure of proteins in crystalline state is determined by single-crystal X-ray diffraction. In aqueous solution, these macromolecules are expected to have nearly the same structure as in crystalline state. Many native proteins (in pure state) exhibit a globular overall shape but conformational changes (folding/unfolding processes) may occur when an organic solvent or other type of molecules are added to the solution or when the pH is modified. Proteins only crystallise under very special conditions of purity and pH and so structural studies regarding conformational variations can only be performed in solution state. SAXS is one of the most widely used technique for structural studies of protein/water solutions.

The addition of increasing amounts of an organic solvent, tetramethyurea (TMU), progressively increases the viscosity of lysozyme/water solutions. This effect suggested that TMU addition promotes protein unfolding. Lysozyme/water solutions with different TMU contents were studied by SAXS in order to confirm this hypothesis.

Since the structure function S(q) of concentrated protein/water solutions is not known a priori, it is advisable to perform experimental SAXS studies in dilute systems. Under this condition, S(q) is equal to 1 for all q and so Eq. 3 can be applied. After the preparation of a given solution, the following step should be to verify if the dilution is high enough. However, for dilute solutions, the scattering intensity, particularly at high q, is usually very weak preventing or making SAXS experiments very time consuming using classic X-ray sources. For this reason, SAXS beamlines installed in synchrotron radiation facilities are, at present, widely used for this type of experiments

For native lysozyme solutions (*i.e.* for TMU content w = 0, w is given in mass fraction), the single particle scattering function was calculated (Eq. 2) using the known electronic density function previously determined by single-crystal X-ray diffraction. The calculated scattering intensity function fitted well to the experimental SAXS curve corresponding to the solution without TMU addition, as can be seen in Fig. 4a. The same agreement is apparent in the distance distribution function p(r) defined by Eq. 5 and determined from the experimental scattering function (Fig. 4b). This indicated that the effect of protein concentration on the scattering function is very weak over all q range so that the solution is actually dilute. In order to improve the quality of the experimental scattering function at high q, additional measurements were performed using more concentrated samples. This could be done because the effect of concentration at high q is much less important than in the small q range.

The radius of gyration of native lysozyme was determined by fitting Guinier law (Eq. 6) over the low q range of the experimental scattering function. The obtained value, R_g = 15.2 Å, is similar to that determined from the known atomic structure (R_g = 15.4 Å). The distance distribution function p(r), obtained from experimental scattering function by applying Eq. 5, exhibits a D_{max} value equal to 50.3 Å, in good agreement with D_{max} = 49.6 Å determined from the p(r) function calculated using data of the known atomic structure.

Scattering results corresponding to lysozyme/water/TMU solutions demonstrated that the overall shape

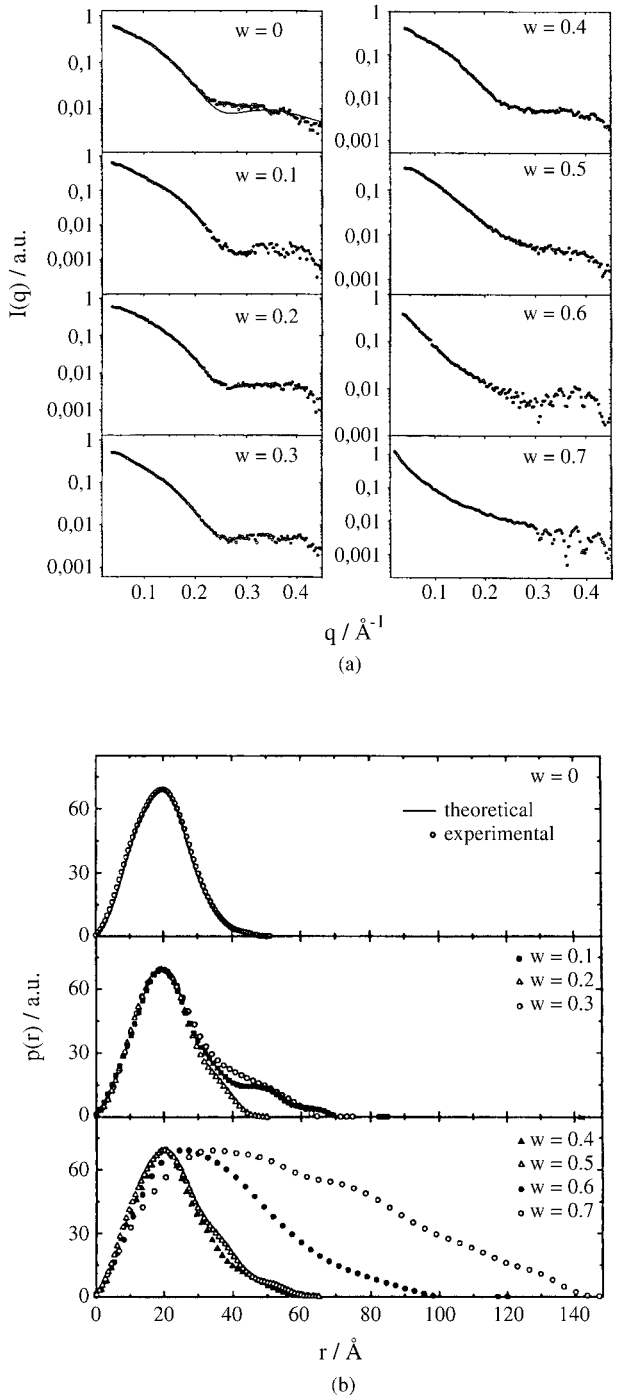

Figure 4. Experimental results corresponding to lysozyme/water solutions with different organic solvent (TMU) contents (w). (a) Scattering functions (b) Distance distribution functions corresponding to the scattering curves shown in (a). Continuous lines in (a) and (b) for w = 0 are the scattering and distance distribution functions, respectively, calculated from the known atomic structure of native lysozyme. Reprinted from Ref. 7 with permission from American Institute of Physics.

of lysozyme varies with TMU content (Fig. 4a and b). For TMU content $w < 0.5$, the maximum diameter D_{max} and the radius of gyration Rg are small and approximately independent of w. For $w \geq 0.6$, R_g and D_{max} increase sharply indicating that the protein molecule becomes highly anisometric. The increase in D_{max} is clearly apparent in Fig. 4b. This effect is a consequence of an unfolding process and explains the results of previously mentioned viscosity measurements.

The next step was to investigate the eventual reversibility of the conformational variation. For that, the added TMU molecules were extracted from the solution. The scattering function of the sample from which the organic solvent was removed was found to be similar to the curve of native lysozyme. This demonstrated that the unfolding/folding process promoted by the addition of TMU is a reversible transformation.

The reported experimental results suggest a model of two different equilibrium states for lysozyme characterised by a folded conformation and an unfolded one, respectively. According to this model, only folded or unfolded states are present in significant concentrations for all TMU content.

5.2. Liquid ZnO suspensions and aggregation processes[8]

Powders composed of ZnO nanoparticles obtained by the sol-gel route are used as precursors for the development of materials with interesting properties. The first step of sol-gel processing leading to ZnO nanoparticles is the formation of a liquid suspension of zinc acetate in ethanol in which LiOH is added under ultrasound treatment. Maintaining the solution inside a cell at a constant temperature, the dissolved molecules start to aggregate, yielding colloidal particles of progressively increasing size.

In order to study the first steps of the aggregation process, an *in situ* SAXS study was performed. The sol was placed inside a cell held at 40 °C with the incident X-ray beam passing through it. The different scattering functions obtained after increasing periods of time where analysed assuming that the system is dilute and that the colloidal particles are nearly spherical. This assumption was confirmed by TEM studies of dried solutions.

In order to determine the size distribution of the colloidal particles, the integral Eq. 11 was solved by using the GNOM package. This numerical procedure was applied to several experimental scattering functions corresponding to different periods of aggregation time, yielding a set of particle volume distribution functions, $D(R) = (4/3)\pi R^3 G(R)$.

The scattering curves corresponding to suspensions held at 40 °C during increasing periods of time are plotted in Fig. 5. The experimental results demonstrate that the kinetics of ZnO colloidal formation is characterised by two main stages. In the first one, a growing peak in D(R) function centred at R = 17 Å is apparent, indicating a

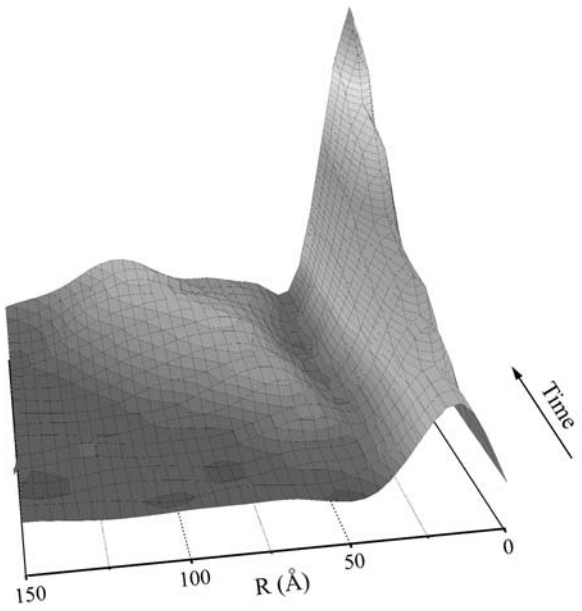

Figure 5. Kinetics of aggregation of ZnO colloidal suspensions in alcoholic solution. Particle volume distribution functions correspond to increasing periods of time, from 10 to 120 min, with the suspension maintained at a constant temperature (T = 40 °C) inside the SAXS sample cell. Reprinted from ref. 8 with permission from Elsevier.

continuous formation of small colloidal particles. The number of these olygomers increases monotonously for increasing reaction time, while their average size remains constant. The nature of zinc-based molecular olygomers in ethanolic solution is not well known but the radius determined by SAXS seems to correspond to the size of the crystallographic unit cell of a zinc acetate derivative compound. This suggests that, initially, polycondensation reaction leads to the formation of trimeric or tetrameric colloidal objects.

In a second stage, the D(R) functions exhibit a still growing peak centred at 17 Å and the appearance and growth of a second peak corresponding to an initial average particle radius R = 60 Å. The peak position shifts continuously toward higher R values up to 110 Å for a period of time of 2 h. These variations in D(R) functions clearly indicate the continuous formation of colloidal primary particles and their simultaneous aggregation and consequent particle growth.

Electron diffraction experiments demonstrated that primary particles are crystalline, with a zinc wurtzite structure, suggesting that they are formed by oxolation reactions involving small olygomers existing in the early time period of synthesis.

The progressive clustering of primary particles leads to the formation of large aggregates exhibiting a fractal structure. Fitting the function given in Eq. 15 to the experimental scattering functions corresponding to long periods of time yields a fractal dimension D = 1.7. This value is close to that expected for a mechanism of growth controlled by diffusion-limited cluster-cluster aggregation.

5.3. Structural transformation in nanoporous NiO xerogels[9,10]

Solutions of alkoxides in alcohol can be destabilised by hydrolysis and polycondensation, promoting the formation of progressively growing aggregates. Under specific conditions, very small (colloidal) particles are formed and stable sols are obtained. Addition of water to the initial solutions promotes the formation and growth of clusters, which eventually establish contacts and bonds between themselves. The aggregation process may be controlled by the mechanism of diffusion of primary species embedded in the liquid phase or by the chemical reaction associated to interparticle bonding. Primary species may aggregate forming progressively growing clusters (particle-cluster aggregation). Also, diffusing clusters may bond between themselves (cluster-cluster aggregation). Depending on the concentration of primary particles, particle-cluster or cluster-cluster aggregation may lead to an infinite sized body, *i.e.* a continuous network occupying all sample volume. This final soft solid is named a gel.

The increasing size of the aggregates progressively increases the viscosity of the sol, which exhibits a sharp rise when sol-gel transition occurs. Gels contain an important amount of solvent inside the pore phase. By extracting the solvent from the "wet" gel, a fine porous powder (a xerogel) is produced. Under special conditions, such as hypercritical drying, monolithic porous gels can also be obtained.

Porous *NiO*-based powdered xerogels were prepared using the sol-gel procedure. The precursor sols were composed of nickel chloride, acetic acid and different amounts of water dissolved in butanol. The liquid solutions were refluxed and the resulting sols dried and held during one hour at different temperatures from 150 up to 900 °C. SAXS measurements were performed on several samples with different acetic acid and water contents in order to characterise the nanoporous xerogels.

The experimental results plotted in Fig 6a demonstrate that, for low-temperature heat-treatments (150 and 300 °C), the scattering functions exhibit a nonlinear behaviour in *log-log* plots. At high temperatures, the logarithm of intensity approaches to a linear dependence on *log q*.

The pore volume distributions corresponding to xerogels heat-treated at different temperatures were determined from the experimental scattering functions using the GNOM package and are plotted in Fig. 6b. It was assumed that the system consists of a non-correlated set of pores modelled by a polydisperse system of hard spheres. The results demonstrated that, for low heat-treatment tempera-

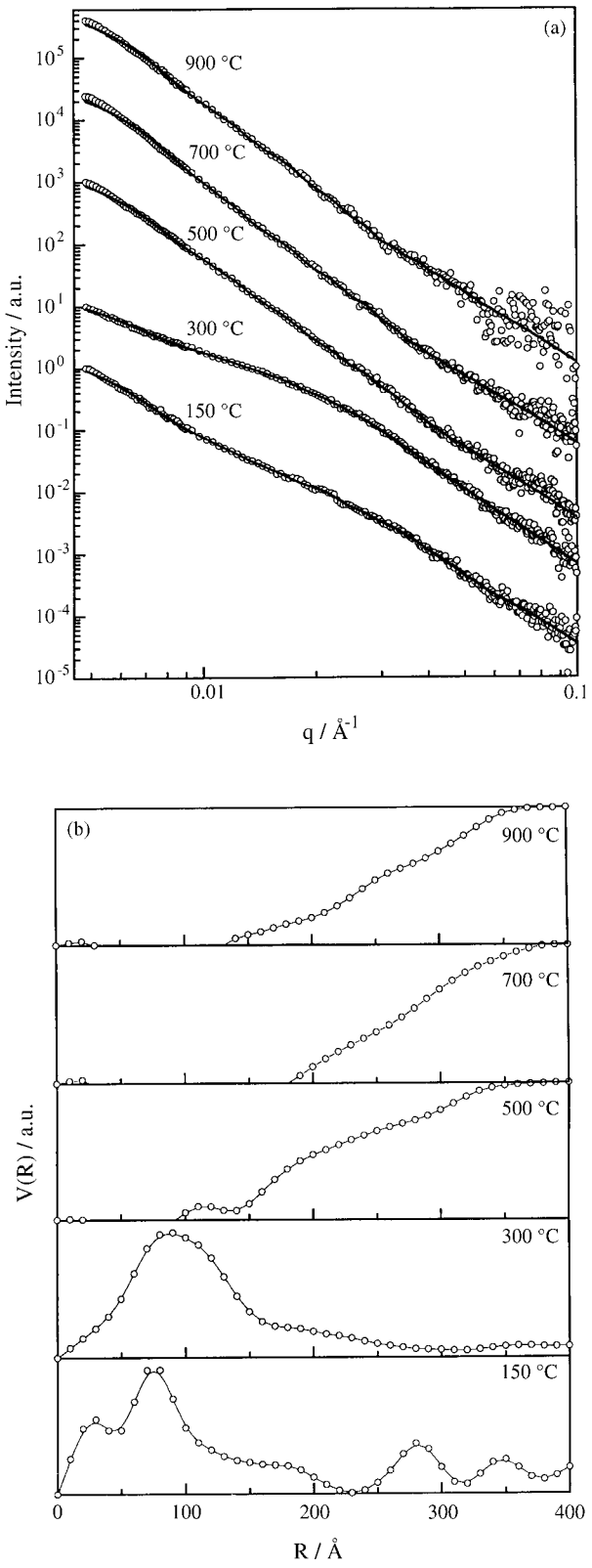

Figure 6. (a) Scattering functions and (b) pore volume distribution function of NiO based porous xerogels heat-treated during 1 h at the indicated temperatures. Reprinted from Ref. 10 with permission from the International Union of Crystallography.

tures (150-300 °C), the pore volume distribution D(R) exhibits a peak centred at R = 75 Å (nanopores). In addition, it indicates a wide distribution of larger pores, with a size continuously ranging from 100 up to 400 Å (mesopores). The highest value of R = 400 Å is associated to the limitation imposed by the existence of a minimum q value in the experimental scattering functions.

The volume distribution function of xerogels heat-treated at temperatures equal to and higher than 500 °C demonstrates the existence of mesopores (R > 100 Å) and the absence of nanopores with R < 100 Å. The same was concluded for all studied xerogels, regardless their water content.

The reported results indicate that, for low heat-treatment temperatures (150-300 °C), xerogels exhibit a nanoporous structure and a minority of mesopores of varying size. The porosity is produced by the evaporation of water and progressive elimination of organic compounds. At higher temperature, the increase in the average size of nanopores is promoted by the progressive elimination of structural water and less volatile organic compounds. An additional effect is the coarsening and coalescence of existing nanopores, thus increasing the number and size of mesopores.

5.4. Hybrid organic-inorganic xerogels: formation and structural properties

5.4.1. Wet gels[11]

The development of nanocomposite materials consisting of two phases, one of them organic and the other inorganic, has recently received the attention of many materials scientists. These hybrids can be designed in such a way as to obtain a composite preserving some of the interesting properties of one of the phases, the second one contributing to improve others. These materials are prepared by sol-gel processing.

Precursor solutions composed of polyethileneglycol (PEG) and polypropyleneglycol (PPG) polymers, with both ends chemically grafted to siloxane molecules, dissolved in ethanol were prepared. After addition of water and stirring, transparent sols were obtained. The aggregation in sol phase and the gelation process were studied by SAXS. The experimental results indicated that siloxane end molecules aggregate leading to clusters exhibiting a fractal structure. Fractal clusters are linked between them by polymeric chains. Fittings of Eq. 15 to the experimental scattering functions yielded the fractal dimension, the aggregate correlation length and their variation with time.

The correlation length, associated to the size of the silica-based fractal aggregates, increases from 60 to 130 Å, while the fractal dimension varies from 2.4 to 2.7. The variation in fractal dimension indicates that the growth of

aggregates is not controlled by a single mechanism. The results suggest that, simultaneously to aggregate growth, an internal rearrangement, or ageing, occurs.

5.4.2. Dry gels[12]

Dry gels containing siloxane-grafted PEG and PPG polymers with different molecular weight (or chain length) were studied by SAXS. Scattering spectra from all of them exhibited a well-defined peak, the q value corresponding to the maximum increasing for decreasing polymer chain length. This trend led us to the conclusion that the observed peak in scattering intensity functions is a consequence of interference effects on X-ray scattering amplitude produced by spatial correlation of closely located SiO_2 - based clusters embedded in the polymeric matrix.

5.4.3. Drying process[11]

The drying process of siloxane-grafted PPG wet gels was studied in situ by SAXS. Drying was achieved by opening the cell containing the initially wet gel. The open cell was maintained at a constant temperature (T = 70 °C) during in situ SAXS measurements. The scattering functions of partially dried samples plotted in Fig. 7 exhibit a peak at q = 0.15 $Å^{-1}$ with a maximum intensity increasing for increasing periods of time. The average distance between aggregates, estimated from the position of the scattering peak by using Eq. 14, was d_s = 42 Å. The low value of the average interaggregate distance (smaller than the radius of gyration of the fractal silica aggregates in the precursor wet gels) indicated that both, fractal aggregates and polymeric matrix, shrink during the drying process.

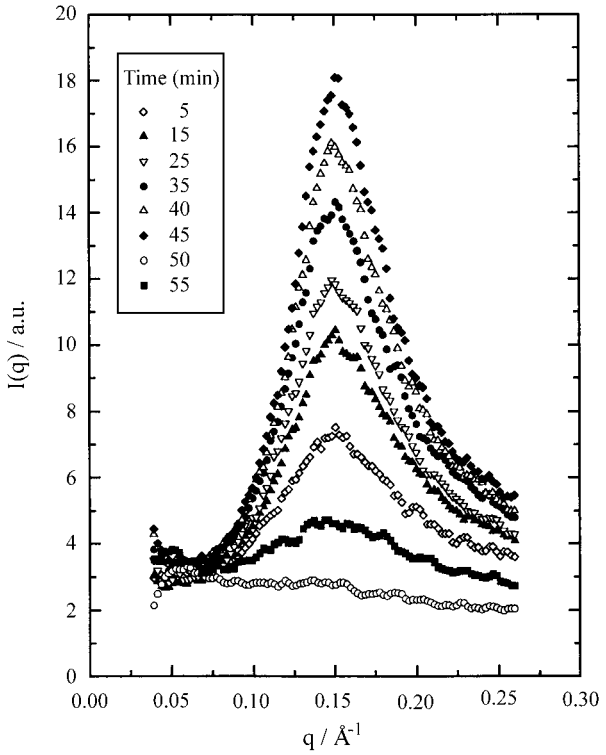

Figure 7. Scattering functions of PPG-siloxane grafted hybrids obtained during the drying process at 70 °C. Reprinted from Ref. 11 with permission from Japanese Journal of Applied Physics.

The constant position of the progressively growing peak of the experimental scattering function (Fig. 7) and, consequently, the invariance of average interparticle distance d_s suggested that the drying process can be described as a first-order phase transition. The basic conclusion was that the drying plate-shaped sample consists of (i) two well-defined dry layers of increasing thickness, close to the both external surfaces, and (ii) a remaining wet layer in the central part. The increase in scattering intensity, as drying goes on, would be a consequence of the progressive increase in volume fraction of the dry phase.

5.4.4. Effects of Li salt addition[13]

The effect of addition of Li salt on the structure of siloxane grafted PEG hybrids was also studied by SAXS. Experimental scattering curves corresponding to several Li contents exhibit a correlation peak with different maximum intensity values.

For low-doped samples, the peak position q_m and, consequently, the interparticle average distance between silica clusters, d_S, (Eq. 18) remain invariant as doping increases. The decrease observed in the integral Q (Eqs. 12 and 13) was attributed to a decrease in electronic density contrast, ρ_1-ρ_0, as a consequence of a progressive filling effect of the increasing amount of Li^+ interacting with the ether-type oxygens and occupying the open space between polymeric chains.

For intermediate doping level, a decrease in interparticle spacing d_S and in the integral Q for increasing Li^+ content were observed. The decrease in d_s suggests a contraction of the polymer structure as a consequence of the increase in degree of cross-linking O-Li^+-O between polymeric chains. On the other hand, the contraction of polymeric phase increases its electronic density so reducing the contrast between the electronic density of the two phases (ρ_1 - ρ_0). This justifies the decreasing tendency of the integral Q.

For high-doping level, the structure of the polymeric phase becomes more and more contracted because of the increase in the cross-linking degree, as suggested by the decrease in d_s. The contraction is high enough to induce a noticeable increase in silica-rich volume fraction ϕ. At the same time, the polymer electron density ρ_0 increases as a consequence of the contraction in polymeric phase. These two simultaneous phenomena explain small variations observed in the integral Q (Eq. 12).

The proposed structural model is consistent with the behaviour of ionic conductivity at room temperature. It is well established that, in polymer electrolytes, ionic conduction occurs in the polymeric phase of the material. For pure PEG and PPG polymers and low Li salt addition, the increase in conductivity is simply due to the increasing number of cations. For high salt content, the decrease in conductivity after the maximum is attributed to the formation of cross-linking O-Li^+-O between oxygen atoms of different polymer chains, leading to an increase in chain rigidity.

5.5. Formation and growth of nanocrystal in glass composites[14]

Doped glasses containing semiconductor nanocrystals exhibit non-linear optical properties, making them good candidates for telecommunication devices. The properties of these materials are particularly interesting when nanocrystals are spherical and have a narrow radius distribution.

A doped silicate glass initially containing Pb and Te ions was investigated by SAXS in order to determine the shape, size and size distribution of PbTe nanocrystals and characterise their formation and mechanism of growth under isothermal condition.

The precursor doped glass was quenched from high temperature by means of the splat-cooling technique using two metallic blocks driven one against the other by the action of a strong spring. Thin 100 μm-thick lames, close to the optimum thickness for SAXS experiments, were obtained. The sample was then held at a constant temperature, T = 650 °C, inside a high-temperature cell installed at a synchrotron SAXS beamline for *in situ* measurements.

The experimental scattering functions corresponding to different heat treatment times at constant temperatures are plotted in Fig. 8. The scattering intensity produced by nanocrystals progressively grows and exhibits an oscillation and secondary maximum at high q values. This maximum is not clearly apparent in the early stages of crystal growth because of the rather high statistical errors in scattering intensities. The position and intensity of the observed secondary maximum are qualitatively consistent with the theoretical prediction for a set of identical spheric particles (Eq. 10). The observed small deviations of experimental scattering function from the theoretical one (Eq. 10) suggest that PbTe nanocrystals are spherical and have a narrow size distribution.

As can be seen in Fig. 8, the theoretical scattering functions of a dilute set of growing spheres with a Gaussian radius distribution (Eq. 11) fit very well to all experimental curves. The positive deviations of the experimental scattering functions from the theoretical ones at extremely low q

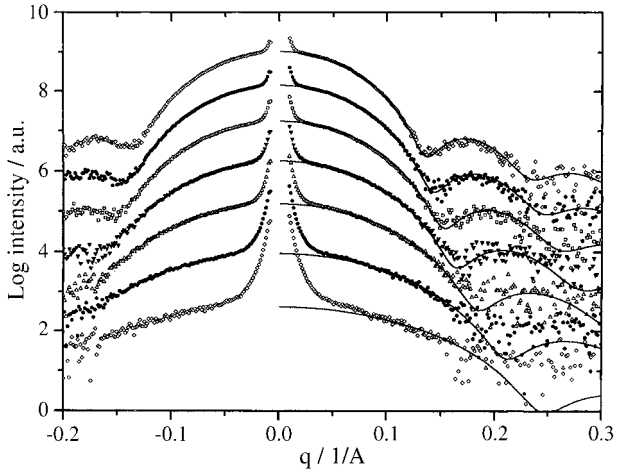

Figure 8. Scattering functions of PbTe nanocrystals embedded in a silicate glass matrix held at a constant temperature (650 °C) for different periods of time from 10 to 120 min. The sample was placed inside a high temperature cell during in situ SAXS measurements. The curves were vertically displaced for clarity. Reprinted from Ref. 14 with permission from the International Union of Crystallography.

were attributed to the existence of coarse heterogeneities in the glass matrix. The fittings of Eq. 11 to the different experimental SAXS curves yielded the values of the average radius, the variation in the number of nanocrystals and the parameter σ characterising the width of the Gaussian radius distribution. The average nanocrystal radius increases from 15 to 33 Å for periods of time of isothermal treatment increasing from 0 to 120 min. The parameter σ varies in such a way that the quotient σ/<R> remains constant and equal to 10% during the whole process of crystal growth.

The average radii of the nanocrystals were independently calculated using experimental optical absorption data and a simple theory that assumes identical spheric nanocrystals and a parabolic dependence of energy E on wave-number k of conduction electrons (Efros and Efros theory). For a number of other studied nanocomposites, this theory yielded reasonably good estimates of nanocrystal radii. However, the nanocrystal radii of PbTe nanocrystals derived from SAXS experiments and those determined from optical spectroscopy did not agree. This demonstrates that not all the simple assumptions of Efros and Efros theoretical model, namely that regarding the function E(k), apply to PbTe nanocrystals.

6. Final Remarks

The reviewed investigations are examples of application of the SAXS technique using synchrotron radiation to structural characterisation of a number of different nanomaterials and colloidal solutions. They also illustrate the usefulness of the knowledge of the structure at a supera-

tomic level for a better understanding of many materials properties.

The photon flux of the LNLS synchrotron source is maximum for energies close to 1 keV (Fig. 1), not so being optimised for the emission of 8 keV photons ($\lambda \sim 1.5$ Å) often employed in SAXS experiments. Nevertheless, the experimental SAXS results reported here demonstrate that the flux of 8 keV photons is high enough to make a number of interesting studies on the structure of solutions, gels and solid materials possible. It also permits the investigation of structural transformations, from precursors to final materials, with a resolution time on the order of one minute.

It is also worth mentioning that all reviewed studies were performed using a nearly "pin-hole" geometry for the incident beam. This geometry is convenient because, under this condition, experimental scattering functions do not need to be desmeared using mathematical procedures, so increasing the accuracy of the structural information obtained from data analysis.

Acknowledgment

The author thank all the collaborators and graduate students that participated in the reviewed investigations. They are cited in references 1 to 3 and 7 to14. Most of them are frequent LNLS users and currently work at Institute of Chemistry (UNESP), Institute of Chemistry and Institute of Physics (UNICAMP), Institute of Chemistry and Institute of Physics (USP) and National Synchrotron Light Laboratory (LNLS), research institutions located in Sao Paulo State, Brazil. SAXS experiments were performed at LNLS except the reported in section 5.5, which were carried out at LURE (Orsay, France). The author also acknowledges the assistance of the staff of these two synchrotron laboratories during SAXS experiments.

References

1. Rodrigues, A.R.D.; Craievich, A.F.; Gonçalves da Silva, C.E.T. *J. Synchr. Rad.*, v. 5, p. 1157, 1998.
2. Tavares, P. *Private communication*, 2002.
3. Kellermann, G.; Vicentin, F.C.; Tamura, E.; Rocha, M.; Tolentino, H.; Barbosa, A.F.; Craievich, A.F.; Torriani, I. *J. Appl. Cryst.*, v. 30, p. 880, 1997.
4. Glatter, O.; Kratky, O. *Small-Angle X-ray Scattering*, Academic Press, New York, 1982.
5. Svergun, D.I. *J. Appl. Cryst.*, n. 25, p. 495, 1992.
6. Teixeira, J. *J. Appl. Cryst.*, v. 21, p. 781, 1988.
7. Castelleto, V.; Areas, E.P.G.; Areas, J.A.G.; Craievich, A.F. *J. Chem. Phys.*, v. 109, p. 465, 1998.
8. Tokumoto, M.S.; Pulcinelli, S.H.; Santilli, C.V.; Craievich, A.F. *J. Non-Cryst. Solids*, v. 247. p. 176, 1999.
9. Fischer, H.; Sharma, P.K.; Craievich, A.F. *J. Amer. Ceram. Soc.*, v. 82, p. 1020, 1999.
10. Fischer, H.; Sharma, P.K.; Craievich, A.F. *J. Appl. Cryst.*, v. 33, p. 478, 1999.
11. Dahmouche, K.; Santilli, C.V.; Chaker, J.A.; Pulcinelli, S.H.; Craievich, A.F. *Japan. J. Appl. Phys.*, v. 38, n. 1, p. 172, 1999.
12. Dahmouche, K.; Santilli, C.V.; Pulcinelli, S.H.; Craievich, A.F. *J. Phys. Chem. B*, v. 103, p. 4937, 1999.
13. Dahmouche, K.; Santilli, C.V.; da Silva, M.; Pulcinelli, S.H.; Craievich, A.F. *J. Non-Cryst Solids*, v. 247, p. 108, 1999.
14. Craievich, A.F.; Alves, O.L.; Barbosa, L.C. *J. Appl. Cryst.*, v. 30, p. 623, 1997.

FAPESP helped in meeting the publication costs of this article